IEEJ Journal of Industry Applications
Vol.10 No.1 pp.1–10 DOI: 10.1541/ieejjia.19012766

Paper

Position Sensorless Adaptive Positioning Servo System with Simplified Differential Calculation and High-Frequency Voltage Injection Strategy Considering Acoustic Noise Suppression

Naoki Kawamura* Student Member, Tadanao Zanma* Senior Member
Kenta Koiwa* Member, Kang-Zhi Liu* Member
Masaru Hasegawa** Senior Member

(Manuscript received Nov. 22, 2019, revised March 2, 2020)
J-STAGE Advance published date : Oct. 1, 2020

In position sensorless positioning servo systems, the parameter mismatch between interior permanent magnet synchronous motors (IPMSMs) and a position controller and/or a position estimator due to thermal variation and aged deterioration has not been sufficiently investigated. This paper proposes a convolutional integration-based second-order differential calculation to identify the parameters of IPMSMs for a high-performance positioning servo system in an adaptive scheme. In addition, we propose a high-frequency voltage injection strategy considering the trade-off between acoustic noise suppression and estimation performance. The effectiveness of the proposed second-order differential calculation calculation method, and the high-frequency voltage injection for the acoustic noise suppression is verified experimentally.

Keywords: position sensorless control, positioning servo system, adaptive control, convolutional integration-based-differential calculation, and acoustic noise suppression

1. Introduction

Positioning servo systems of interior permanent magnet synchronous motors (IPMSMs) with position sensors such as encoders or resolvers have been widely used in many applications. Since the position sensor increases cost and dimension, position sensorless control for positioning servo systems has been developed [1]–[5].

An accurate position estimation is indispensable in the position sensorless positioning servo systems. Since the estimator is designed using the parameters of the IPMSM, it is necessary to identify the parameters that vary according to environmental changes in estimation. The adaptive scheme is suitable for an automatic parameter identification since the stability can be analyzed only using the phase characteristics of the system. We have proposed an adaptive position controller [6][7] and a comb filter-based position estimator [8], in which the second-order differential of the identified parameters is needed for control input. For the differential calculation, an high-order tuner (HOT) is generally used in the adaptive scheme [9]. HOT requires a heavy computational burden which causes the control delay. In addition, the upper bound of the high-frequency gain of the controlled plant is assumed to be known in advance in HOT for stabilization. Although a convolutional integration based-differential calculation method with a relatively low computation cost has been proposed in [10][11], the control delay is still inevitable.

To overcome the control delay resulting from the differential computation, we propose a simplified differential calculation of augmented parameters in the adaptive scheme by refining the basic ideas [12][13]. By the proposed method, the high-frequency gain can be reduced compared to the backward-Euler-based differentiator, which reduces the influence of measurement noise due to the differential operation. The computational burden can be reduced compared to HOT since the proposed method uses the inner product operation only.

For the position estimation in the position sensorless positioning servo systems, the high-frequency voltage injection [14][15] is suitable rather than the back electromotive force (EMF) [16] since a sufficient back EMF is not available at a standstill (including zero speed) or in very low speed ranges. In fact, a multiple space vector pulse width modulation (SVPWM) [1], a high-frequency pulse-voltage injection [3], an adaptive flux observer with high-frequency pulse-current injection [4], and a pulse voltage injection [2][5] have been introduced for the position estimation. These can be regarded as a kind of the high-frequency voltage injection methods, which causes acoustic noise in operation. To suppress the acoustic noise, a variable voltage amplitude injection according to q-axis current [17], an adaptive amplitude and frequency of the injected voltage [18], and a frequency spreading of the injected voltage method [19][20] have been proposed. Although the acoustic noise can be suppressed by theses methods, position estimation performance deteriorates due to q-axis current

* Graduate School of Engineering, Chiba University
1-33, Yayoi, Inage, Chiba 263-8522, Japan
** Department of Electrical and Electronic Engineering, Chubu University
1200, Matsumoto, Kasugai, Aichi 487-8501, Japan

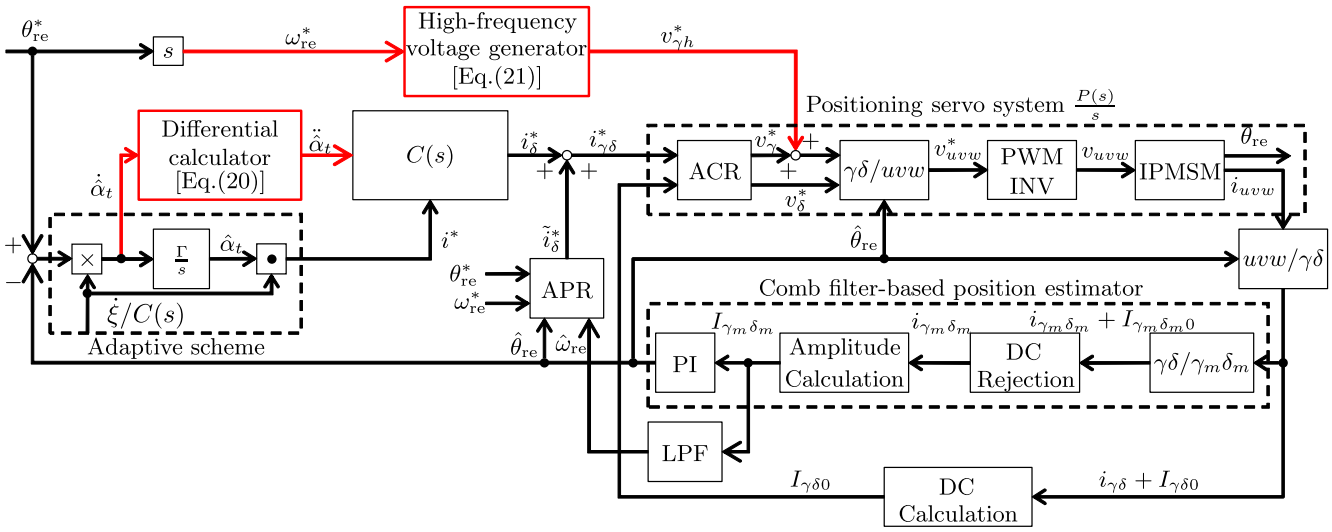

Fig. 1. Block diagram of position sensorless adaptive positioning servo system

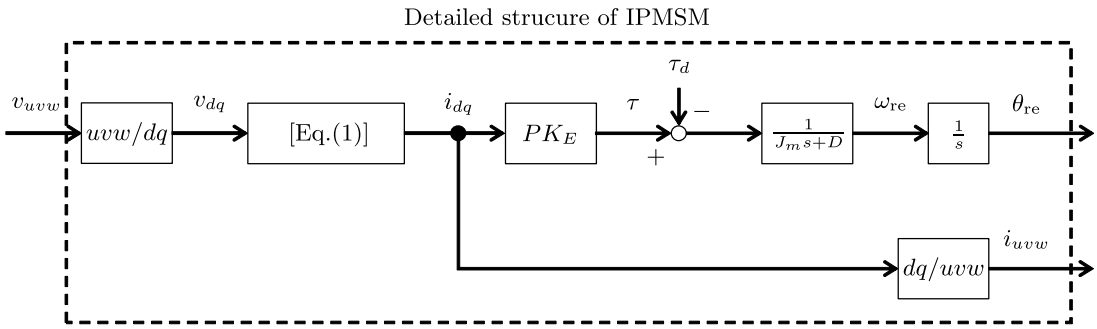

Fig. 2. Detailed structure of IPMSM

oscillation [17], measurement noise of the current [18], and a low superimposing-frequency voltage [19][20].

Considering this inevitable trade-off between the acoustic noise suppression and the estimation performance, we also propose a high-frequency voltage injection strategy to suppress the acoustic noise for position estimation by refining the basic idea [13]. The proposed method also has DC disturbance rejection characteristics which has not been clearly addressed [17][18]. In the proposed method, the superimposed voltage amplitude for the acoustic noise suppression is variable in accordance with the speed reference, so that the robustness to measurement noise can be improved. The transient state and the steady state are distinguished by means of the speed reference obtained by the minimum jerk trajectory. Since the variable voltage amplitude can be expressed as a linear function of the speed reference, its implementation cost is low.

The effectiveness of the proposed the second-order differential calculation of the identified parameters for the position estimation, and the high-frequency voltage injection for the acoustic noise suppression are verified through experiments.

This paper is organized as follows: Section 2 describes the position sensorless positioning servo systems, the rotor position estimator by using the comb filter, and the adaptive positioning servo system with control input synthesis. In Section 3, we propose a convolutional integration-based differential calculator, and a high-frequency voltage injection for acoustic noise suppression. Section 4 shows the effectiveness of the proposed strategies via experiments, focusing on positioning control performance and acoustic noise suppression. Section 5 concludes this paper.

2. Position Sensorless Positioning Servo System

Figure 1 shows the position sensorless positioning servo system considered in this paper. This system consists of the comb-filter-based position estimator, PI controller-based automatic current regulator (ACR), PD controller-based automatic position regulator (APR) and the adaptive scheme.

For a signal $x(t)$ in the time domain, its Laplace transform is denoted by $x(s)$ in the frequency domain. In addition, the Laplace transform of $\dot{x}(t)$ is denoted by $\dot{x}(s)$ instead of denoting $sx(s)$ when we need to emphasize the Laplace transform of $\dot{x}(t)$ itself which is applicable when $\dot{x}(t)$ is available directly or observable. For a signal $x(t)$ (typically, voltage, current, rotor position), $\hat{x}(t)$ and $x^*(t)$ denote the estimated value and the reference of $x(t)$, respectively.

Table 1 lists the symbols used in this paper.

2.1 Rotor Position Estimation for IPMSMs

We focus the position sensorless positioning servo system operated at a standstill ($\omega_{\rm re} = 0$) or a very low speed ($\omega_{\rm re} \simeq 0$).

The back EMF-based position sensorless control fails to operate at a standstill and the very low speed operation since the back EMF is hard to obtain under such operating conditions.

The voltage equation of IPMSM is represented as

Table 1. Notations

Parameter	Symbol	Unit
Stator resistance	R	Ω
d-axis inductance	L_d	H
q-axis inductance	L_q	H
Back-EMF Constant	K_E	Vs/rad
Number of Pole Pairs	P	-
Rotor position	$\theta_{\rm re}$	rad
Rotor speed	$\omega_{\rm re}$	rad/s
Stator voltage vector	$v_{dq} = \begin{bmatrix} v_d & v_q \end{bmatrix}^\top$	V
Stator current vector	$i_{dq} = \begin{bmatrix} i_d & i_q \end{bmatrix}^\top$	A
Inertia	$J_{\rm m}$	kgm^2/s^2
Friction coefficient	D	Nms

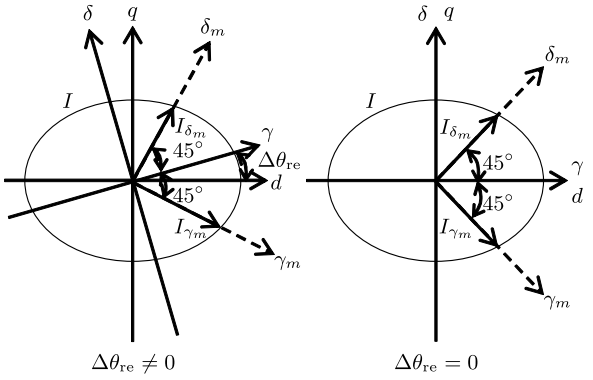

Fig. 3. High-frequency current vector of IPMSM

$$\begin{bmatrix} v_d \\ v_q \end{bmatrix} = \begin{bmatrix} R & 0 \\ 0 & R \end{bmatrix} \begin{bmatrix} i_d \\ i_q \end{bmatrix} + \frac{d}{dt} \begin{bmatrix} L_d & 0 \\ 0 & L_q \end{bmatrix} \begin{bmatrix} i_d \\ i_q \end{bmatrix} + \left(\begin{bmatrix} 0 & -\omega_{\rm re} L_d \\ \omega_{\rm re} L_q & 0 \end{bmatrix} \right) \begin{bmatrix} i_d \\ i_q \end{bmatrix} + \begin{bmatrix} 0 \\ \omega_{\rm re} K_E \end{bmatrix}. \quad \cdots\cdots (1)$$

Assuming L_d and L_q are constant at a standstill or a very low speed, we can ignore the last two terms in rhs of (1). Thus, the back EMF-based rotor position estimation fails since only the fundamental component of the current $\boldsymbol{i}$ is available. Hence, the high-frequency voltage injection is used to excite the magnetic saliency due to the rotor structure of an IPMSM so that the rotor position is estimated at a standstill and a very low speed.

The high-frequency current trajectory is ellipsoidal as shown in the left-hand side of Fig. 3 since $L_d < L_q$ in general. In Fig. 3, γ-δ_m axes are defined at 45° from γ-δ axes (the estimated d-q axes). The amplitude of the high-frequency current shown in Fig. 3 includes information related to the rotor position. In this estimation, no estimation errors exists in the rotor position when $I_{\gamma_m} = I_{\delta_m}$. Consequently, the rotor position is successfully estimated when $I_{\delta_m} - I_{\gamma_m}$ converges to 0 with the PLL [21]. We use the comb filters [22] to obtain I_{γ_m} and I_{δ_m} for a faster rotor position estimation. The comb filter requires only the summation and the delay calculation, and thus, is easy to implement.

2.2 Adaptive Positioning Control System In the earlier positioning control systems [6][8], the positioning controller is composed of a feedforward speed controller including an ACR, a PI-type automatic speed regulator (ASR) and the adaptive scheme (See Appendix for the details). The PI-type ASR shown in Fig. 4(a) causes the control delay due to the integrator in it. In the proposed system shown in Fig. 1, the APR shown in Fig. 4(b) is introduced instead of the

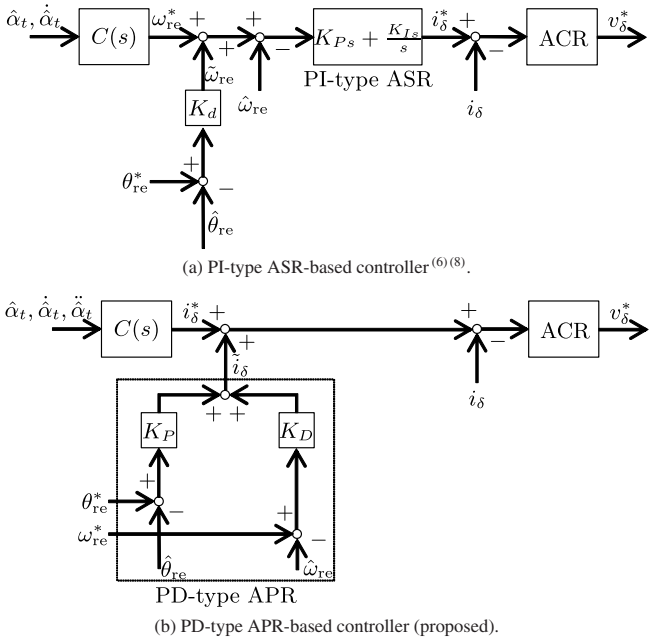

(a) PI-type ASR-based controller [6][8].

(b) PD-type APR-based controller (proposed).

Fig. 4. Block diagram of position controller

PI-type ASR so that the output of the adaptive scheme is connected to the input of the ACR directly, for the high-speed positioning control. As a result, the positioning control performance in the proposed system is characterized by the time constant of the ACR.

Denoting the transfer function from the current reference i^* to the rotor speed $\omega_{\rm re}$ in the positioning servo system as the second-order system $P(s)$ when $C(s) = 1$, we obtain the transfer function from i^* to the rotor position $\theta_{\rm re}$ as $\frac{P(s)}{s}$ by integrating $P(s)$. This transfer function can be formulated as a third-order system [6][8][12][13]:

$$\frac{P(s)}{s} = \frac{\theta_{\rm re}(s)}{i^*(s)} = \frac{1}{s(\alpha_{2t} s^2 + \alpha_{1t} s + \alpha_{0t})}. \cdots\cdots (2)$$

If the time-varying parameters α_{0t}, α_{1t} and α_{2t} vary much more slowly than the current response, the feedforward compensator $i^*(s)$ should be ideally given by

$$i^*(s) = \alpha_{2t} \ddot{\omega}^*_{\rm re}(s) + \alpha_{1t} \dot{\omega}^*_{\rm re}(s) + \alpha_{0t} \omega^*_{\rm re}(s), \cdots\cdots (3)$$

where $\omega^*_{\rm re}$ is the speed reference. In (3), it is necessary to identify α_{0t}, α_{1t}, and α_{2t} in the adaptive scheme. For a higher positioning control performance, we consider the disturbance torque, which has not been addressed in the earlier works [13]. If we assume that the disturbance torque $\tau_d(s)$ is constant, then we rewrite (3) by adding the disturbance term as follows:

$$i^*(s) = \alpha_{2t} \ddot{\omega}^*_{\rm re}(s) + \alpha_{1t} \dot{\omega}^*_{\rm re}(s) + \alpha_{0t} \omega^*_{\rm re}(s) + \frac{1}{PK_E} \tau_d(s). \cdots\cdots (4)$$

In steady state, assuming that $\tau_d(s) = \frac{\tau^c_d}{s}$ and $\theta^*_{\rm re}(s) = \frac{\theta^{*c}_{\rm re}}{s}$ for constants τ^c_d and $\theta^{*c}_{\rm re}$. In this case, we have to determine the unknown parameter vector $\alpha_t = \begin{bmatrix} \alpha_{2t} & \alpha_{1t} & \alpha_{0t} & \tau^c_d \end{bmatrix}^\top$. The

transfer function of APR is supposed to be given by

$$G_{\mathrm{APR}}(s) = sK_D + K_P, \cdots\cdots (5)$$

where $K_D,\ K_P > 0$.

We assume that the ACR is designed such that the transfer function from i^* to i is given by

$$G_{ii^*}(s) = \frac{1}{T_c s + 1}, \cdots\cdots (6)$$

where $T_c > 0$ is a desired time constant of the current control performance.

In this system, the sensitivity function from τ_d to θ_{re} under the assumption of $i^* = 0$ can be described as:

$$\theta_{\mathrm{re}}(s) = \frac{1}{s(J_m s + D)}[\,-\tau_d(s) + PK_E G_{ii^*}(s) G_{\mathrm{APR}}(s)(\theta^*_{\mathrm{re}}(s) - \theta_{\mathrm{re}}(s))]. \cdots\cdots (7)$$

From (5), (6), and (7), we obtain

$$\theta_{\mathrm{re}}(s) = \frac{-(T_c s + 1)\tau_d(s) + PK_E K_P \theta^*_{\mathrm{re}}(s)}{s(J_{\mathrm{m}} s + D)(T_c s + 1) + PK_E(sK_D + K_P)}. \cdots\cdots (8)$$

Using the final value theorem, we obtain

$$\theta_{\mathrm{re}}(t)\,|_{t=\infty} = \frac{-1}{PK_E K_P}\tau_d^c + \theta^{*c}_{\mathrm{re}}. \cdots\cdots (9)$$

In this system, the relative degree of $\dfrac{P(s)}{s}$ is three. The convergence of the identified parameters are not guaranteed [23] since the passivity is not satisfied in this system. By contrast, in the proposed adaptive scheme, the convergence issue is avoided under the assumption that $\hat{\alpha}_t$ varies much more slowly than the other electrical variables.

To recover the relative degree of the plant, the adaptive scheme in this paper is constructed by

$$i^*(s) = C(s)\left[\hat{\alpha}_t^\top \left(\frac{1}{C(s)}\dot{\xi}(s)\right)\right], \cdots\cdots (10)$$

where $C(s)$ is an additional polynomial and $\xi := [\dot{\omega}^*_{\mathrm{re}}\ \ \omega^*_{\mathrm{re}}\ \ \theta^*_{\mathrm{re}}\ \ 1]^\top$. Hence, the transfer function from i^* to θ_{re} of the feedforward path in Fig. 1 becomes $C(s)\frac{P(s)}{s}$, which solves the relative degree issue. In addition, positioning control performance in the transient state can be improved since the time-varying behavior of $\hat{\alpha}_t$ is considered in (10) explicitly. Thus, the adaptive scheme approach enables us to satisfy both the parameter identification stability and transient control performance.

When $C(s) = s(Ks + 1)$ $(K > 0)$ in (10), using the swapping lemma [24], we can rewrite (10) by considering the time-varying variable $\hat{\alpha}_t$ as follows:

$$u(s) = K\ddot{\hat{\alpha}}_t^\top \frac{1}{Ks+1}\xi(s) + \dot{\hat{\alpha}}_t^\top \left(2\xi(s) - \frac{1}{Ks+1}\xi(s)\right) + \hat{\alpha}_t^\top \dot{\xi}(s). \cdots\cdots (11)$$

In the integral-type adaptive scheme shown in Fig. 1, $\dot{\hat{\alpha}}_t$ in (11) can be obtained as $\frac{\dot{\xi}}{C(s)}\Delta\theta_{\mathrm{re}}$, where $\Delta\theta_{\mathrm{re}} = \theta^*_{\mathrm{re}} - \hat{\theta}_{\mathrm{re}}$, whereas $\ddot{\hat{\alpha}}_t$ cannot be obtained directly. Thus, the differential calculation is needed to obtain $\ddot{\hat{\alpha}}_t$.

In HOT that is generally used in the adaptive scheme, $\dot{\hat{\alpha}}_t$ and $\ddot{\hat{\alpha}}_t$ are calculated internally in the process of calculating $\hat{\alpha}_t$. The derivative order of $\hat{\alpha}_t$ is equal to the order of $C(s)$. Since the order of $C(s)$ should be two for stabilizing $C(s)\frac{P(s)}{s}$ in the proposed servo system, it is not impossible to obtain $\ddot{\hat{\alpha}}_t$ by using HOT in principle. However, the computation delay is not negligible due to the integrators in HOT, which is a disadvantage compared with the integral-type adaptive scheme. In addition, the infinity norm of $\frac{P(s)}{s}$ (i.e., $\|\frac{P(s)}{s}\|_\infty$) must be known for stabilization in HOT. Since the actual parameters α_t are unknown, $\|\frac{P(s)}{s}\|_\infty$ is also unknown. As a result, it is hard to guarantee the stabilization in advance when HOT is used in the proposed servo system. For the above reasons, we propose a second-order differential calculation to obtain $\ddot{\hat{\alpha}}_t$ in (11) in the next section.

3. Proposed Method

In this section, we propose a differential calculation for the identified parameters for the rotor position estimation, and a high-frequency voltage injection for the acoustic noise suppression.

3.1 Differential Calculation Based on Convolutional Integration

As described in the previous section, the calculation of $\ddot{\hat{\alpha}}_t$ with HOT causes the computation delay, and thus HOT is not adopted in the proposed servo system. Hence, we propose a second-order differential calculation of it using the convolutional integration for the control input synthesis [10][11].

Assumption 1 For an integer $N > 1$, consider an arbitrary smooth function $m(t)$ which satisfies 1) $m(t) \neq 0$ in $t \in (0, NT_s)$, 2) $m(0) = m(NT_s) = 0$, 3) first-order differentiable, and 4) $\dot{m}(0) = \dot{m}(NT_s) = 0$.

For an $m(t)$ satisfying Assumption 1, using the integration by parts, we can easily obtain

$$\int_{kT_s - NT_s}^{kT_s} \dot{m}(kT_s - t)x(t)dt = -\int_{kT_s - NT_s}^{kT_s} m(kT_s - t)\dot{x}(t)dt. \cdots\cdots (12)$$

Noticing that the calculation is executed in DSP, we rewrite (12) in the discrete-time form as follows:

$$\sum_{i=1}^{N-1} \dot{m}[N-i]x[k-N+i] = -\sum_{i=1}^{N-1} m[N-i]\dot{x}[k-N+i], \cdots\cdots (13)$$

where $x[k] := x(kT_s)$, $\dot{x}[k] := \dot{x}(kT_s)$, $m[k] := m(kT_s)$, and $\dot{m}[k] := \dot{m}(kT_s)$ for $t = kT_s$ $(k > 0)$. In (13), recalling that $m[N-i]$ and $\dot{m}[N-i]$ $(i = 1, \ldots, N-1)$ are given, and thus can be considered as coefficients of $x[k-N-i]$ and $\dot{x}[k-N-i]$, respectively. From Assumption 1, $m[0] = m[N] = \dot{m}[0] = \dot{m}[N] = 0$. By contrast, $x[k-N-i]$ and $\dot{x}[k-N-i]$ $(i = 1, \ldots, N-1)$ are signals. We can rewrite (13) using z-transform as follows:

$$F_n(z)x(z) = F_d(z)\dot{x}(z), \cdots\cdots (14)$$

where $x(z)$ and $\dot{x}(z)$ are the z-transforms of $x[k]$ and $\dot{x}[k]$, respectively, and

$$F_n(z) = \sum_{i=1}^{N-1} \dot{m}[N-i]z^{-(N-i)}, \cdots\cdots (15)$$

$$F_d(z) = -\sum_{i=1}^{N-1} m[N-i]z^{-(N-i)}. \quad \cdots\cdots (16)$$

Defining

$$F(z) := \frac{F_n(z)}{F_d(z)}, \quad \cdots\cdots (17)$$

we obtain

$$\dot{x}(z) = F(z)x(z). \quad \cdots\cdots (18)$$

We can consider $F(z)$ in (18) as a differentiator of $x[k]$, which means we can obtain that $\dot{x}[k]$ from $x[k]$ through $F(z)$.

Specifically, consider the following function:

$$m(t) = (\cos(\omega_N t) - 1)^2, \quad \cdots\cdots (19)$$

where $\omega_N = \frac{2\pi}{NT_s}$. We can easily check that (19) satisfies all the four conditions of Assumption 1.

For a faster computation, we take into consideration $\dot{m}(t) = -2\omega_N \sin(\omega_N t)(\cos(\omega_N t) - 1)$. Since $\omega_N \gg 1$ (since T_s is usually sufficiently small), $|\dot{m}(t)| \gg |m(t)|$ in the range except the neighborhood of $t = \frac{NT_s}{2}$ where $\dot{m}(t) = 0$. Therefore, in this case, $F_n(z)$ becomes more dominant than $F_d(z)$ in (17). Then, we approximate (17) as $\tilde{F}(z)$ as follows:

$$\tilde{F}(z) := \frac{F_n(z)}{F_{dc}}, \quad \cdots\cdots (20)$$

where $F_{dc} = -\sum_{i=1}^{N-1} m[N-i]$ which is the sum of the coefficients of $F_d(z)$ in (16).

We investigate the frequency characteristics of the proposed differential calculation (17) and (20). Figure 5 shows the bode diagrams of the proposed differential calculator (17) and (20). and other typical differentiators. From Fig. 5, we can see that (20) can be regarded as a differentiator.

The proposed differential calculation is also effective up to 1260 rad/s (200 Hz) so that the numerical instability due to the noises in the high-frequency band can be avoided. Since the main frequency of the reference trajectory used in this paper (as will be described in experiments) is less than 126 rad/s (20 Hz), the proposed differentiator is effective.

As shown in Fig. 1, only $\hat{\alpha}_t$ is available in the adaptive scheme. Using (20), we can obtain $\ddot{\hat{\alpha}}_t$ as long as the change rate of $\ddot{\hat{\alpha}}_t$ is relatively small.

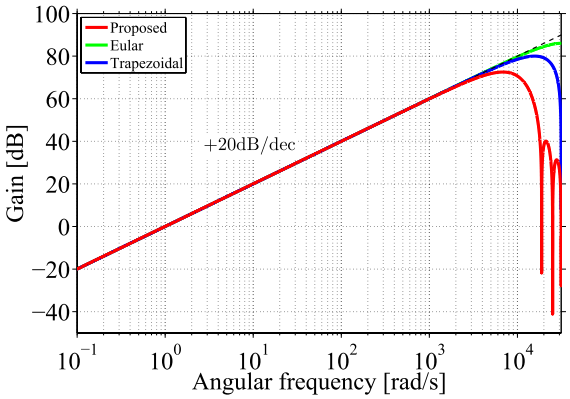

Fig. 5. Bode plots of differentiators

3.2 High-frequency Voltage Injection for Acoustic Noise Suppression Figure 6 shows our experimental environment of an IPMSM servo system. In the experimental setup, a sound level meter, LA-3560 (Ono Sokki), is installed at about 15 cm from the IPMSM. The measurement acoustic pressure level and its frequency range are from 27 dB to 140 dB and from 10 Hz to 20 kHz, respectively. Figure 7 shows the acoustic noise level for the injected high-frequency voltage in 2.5 kHz.

Possible remedies to the acoustic noise are 1) diffusion of the audible components in the injected high-frequency voltage, and/or 2) decrease of the amplitude of the injected high-frequency voltage. The first approach requires several comb filters with different periods. These comb filters have to be switched according to the frequency of the injected high-frequency voltage. These switchings deteriorates the comb-filter-based position estimation. In the second approach, the rotating position estimation performance also degrades when the amplitude of the injected high-frequency voltage not sufficient large. Generally, the amplitude of the injected high-frequency voltage for the position estimation required at transient state is larger than that required at the steady state. In the variable amplitude of the injected high-frequency voltage [17], since the amplitude depends on the q-axis current, the amplitude of the injected high-frequency voltage oscillates, especially at the transient state where the q-axis current increases for positioning control. In addition, the high-frequency voltage is not necessarily injected over the control period.

Thus, we propose a variable high-frequency voltage injection strategy for the acoustic noise suppression. In the strategy, not only the amplitude but also the injection duration is

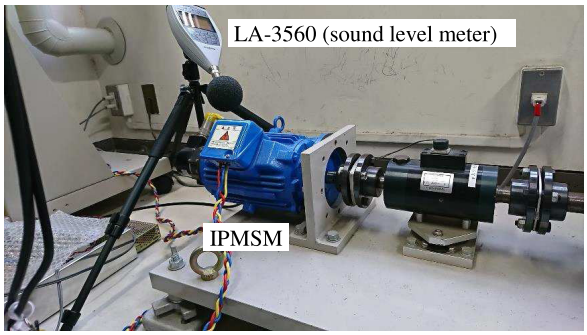

Fig. 6. Experimental environment of IPMSM servo system

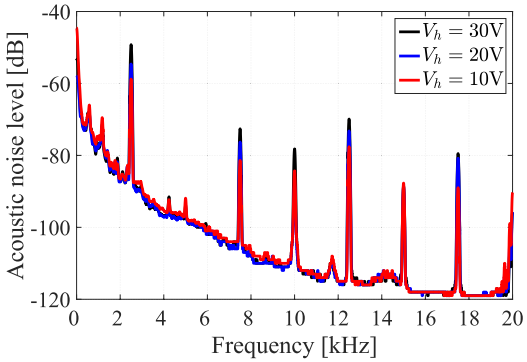

Fig. 7. Acoustic noise levels for different amplitudes of injected high-frequency voltage

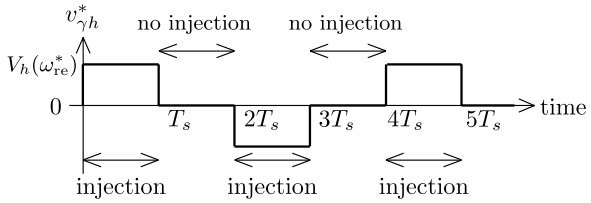

Fig. 8. Injected high-frequency voltage waveform

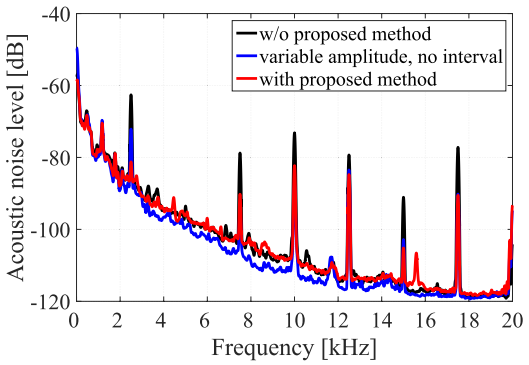

Fig. 9. Acoustic noise suppression effect of proposed high-frequency voltage injection in initial position estimation

considered. Figure 8 shows the injected high-frequency voltage waveform in our strategy.

First, we mention the amplitude of the injected high-frequency voltage. In the positioning servo systems, usually, the position and angular velocity references of the rotor are given in advance [13]. To avoid the oscillation in the injected high-frequency voltage, the angular velocity reference is used instead of the q-axis current. We denote the amplitude of the injected high-frequency voltage as $V_h(\omega^*_{\rm re})$. For a given angular velocity reference $\omega^*_{\rm re}$, the maximum absolute value of $\omega^*_{\rm re}$ is denoted by $\omega^*_{\rm re,max}$. The maximum and minimum values of the injected high-frequency voltage are denoted by $V_{\rm max}$ and $V_{\rm min}$, respectively. Specifically, $V_{\rm max}$ is set due to the upper limit of the injection whereas $V_{\rm min}$ is determined so as to estimate the rotor position at a standstill. To make the use of the injected high-frequency voltage, we set $V_h(\omega^*_{\rm re,max}) = V_{\rm max}$, and $V_h(0) = V_{\rm min}$. For $\omega^*_{\rm re} \in (0, \omega^*_{\rm re,max})$, $V_h(\omega^*_{\rm re})$ is linearly interpolated. Formally, considering the sign of $\omega^*_{\rm re}$, we set the amplitude of the injected high-frequency voltage as follows:

$$V_h(\omega^*_{\rm re}) = \frac{V_{\rm max} - V_{\rm min}}{\omega^*_{\rm re,max}} |\omega^*_{\rm re}| + V_{\rm min}. \cdots\cdots\cdots\cdots (21)$$

Next, we explain the injection duration. As shown in Fig. 8, we introduce the no-injection duration for the injected high-frequency voltage waveform for the acoustic noise suppression. The injection duration should be determined during which the sufficient current evolution can be obtained for the rotor estimation.

Figure 9 shows the acoustic noise suppression effect using the proposed injected high-frequency voltage strategy for the initial position estimation. From Fig. 9, it can be seen that the acoustic noise level can be suppressed about 10 dB by the proposed high-frequency voltage injection, but with no interval in injection. It can also be seen, in Fig. 9, that the acoustic noise level can be further reduced by 9 dB by providing the no-injection duration in the proposed high-frequency voltage injection.

Table 2. Parameters of IPMSM

Parameters	Symbol	Value
Rated power	$P_{\rm n}$	0.75 kW
Rated speed	$\omega_{\rm rmn}$	1750min^{-1}
Rated line voltage	$V_{\rm n}$	143V
Rated line current	$I_{\rm n}$	3.60A
Winding resistance	R	1.14 Ω
d-axis inductance	L_d	12.20 mH
q-axis inductance	L_q	15.96 mH
Back-EMF constant	K_E	0.27V·s/rad
Number of pole pairs	P	3

4. Experiments

This section shows the effectiveness of the proposed position sensorless adaptive positioning servo control of IPMSM. In Fig. 1, $v^*_{\gamma h}$ is the injected high-frequency voltage generated by the injection strategy proposed in the previous section.

Table 2 lists the parameters of the IPMSM. All calculation is executed in a DSP (Texas Instruments incorporated: TM320C6701GJC) installed in the processing board (MTT Corporation: DSP6067). The carrier frequency of the three-phase voltage-type PWM inverter for the IPMSM is 10 kHz. All the controllers and the rotor position estimation are synchronized with the triangular-wave PWM carrier. The control period is 100 μs (i.e., $\frac{1}{10\,\rm kHz}$). The bandwidths of the ACR and the APR are 2000 rad/s and 5 rad/s, respectively. The PWM signal is generated by an FPGA (Field Programmable Gate Arrays).

For the rotating position target L and the moving time T, the position reference is given as follows:

$$\theta^*_{\rm re}(t) = \begin{cases} L\left[6\left(\frac{t}{T}\right)^5 - 15\left(\frac{t}{T}\right)^4 + 10\left(\frac{t}{T}\right)^3\right] & t \in T_{1,l}, \\ L & t \in T_{2,l}, \\ L\left[6\left(\frac{-(t-3T)}{T}\right)^5 - 15\left(\frac{-(t-3T)}{T}\right)^4 + 10\left(\frac{-(t-3T)}{T}\right)^3\right] & t \in T_{3,l}, \\ 0 & t \in T_{4,l}, \end{cases} \cdots\cdots\cdots\cdots (22)$$

where

$$\begin{aligned} T_{1,l} &= [4(l-1)T, 4(l-1)T + T), \\ T_{2,l} &= [4(l-1)T + T, 4(l-1)T + 2T), \\ T_{3,l} &= [4(l-1)T + 2T, 4(l-1)T + 3T), \\ T_{4,l} &= [4(l-1)T + 3T, 4lT), \\ & (l = 1, 2, \ldots). \cdots\cdots\cdots\cdots (23) \end{aligned}$$

In the experiments, $L = 30°$ in the electrical angle (10° in the mechanical angle) and $T = 500$ ms and 250 ms. The angular velocity reference is given as $\omega^*_{\rm re}(t) = \dot{\theta}^*_{\rm re}(t)$, which is used in the proposed high-frequency voltage injection strategy.

4.1 Experimental Results Figures 10 and 11 show the experimental results of the positioning control when $T = 500$ ms and $T = 250$ ms, respectively. In both Figs. 10 and 11, the following conditions are tested: (a) without the differential calculation of $\ddot{\hat{\alpha}}_t$ in the adaptive scheme or the high-frequency voltage injection strategy proposed in Section 3, (b) with only the differential calculation, (c) with both the

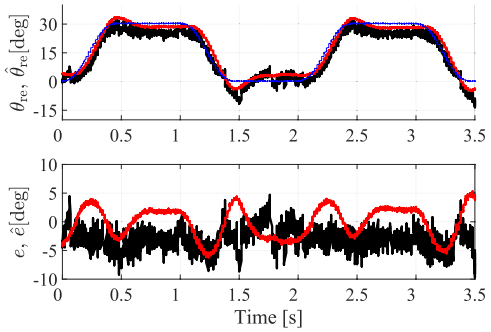

(a) without differential calculation of $\ddot{\hat{\alpha}}_t$ in adaptive scheme or high-frequency voltage injection strategy.

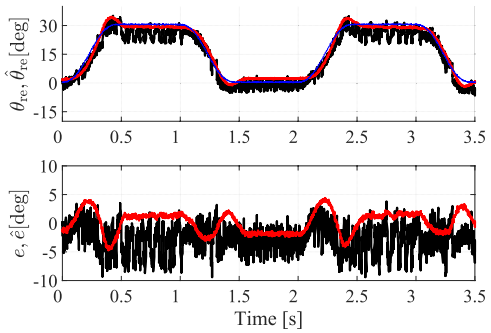

(b) with only differential calculation except τ_d.

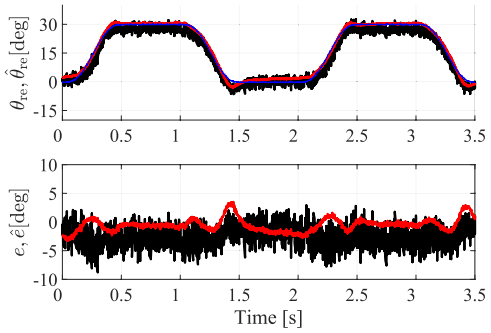

(c) with both differential calculation and τ_d.

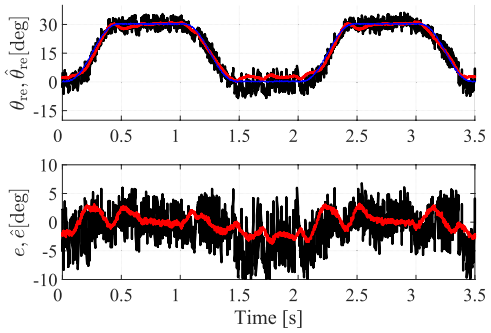

(d) with all proposed strategies.

Fig. 10. Experimental results of positioning control (T = 500 ms)

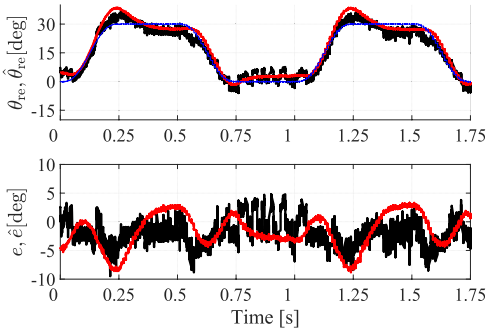

(a) without differential calculation of $\ddot{\hat{\alpha}}_t$ in adaptive scheme or high-frequency voltage injection strategy.

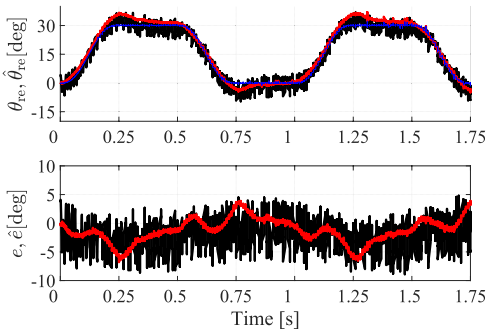

(b) with only differential calculation except τ_d.

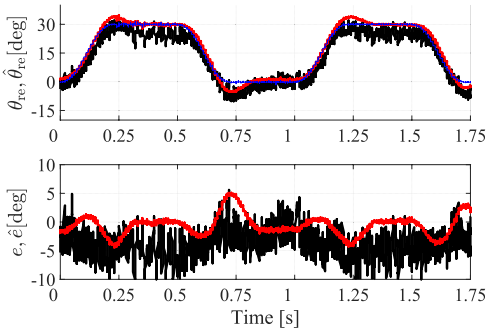

(c) with both differential calculation and τ_d.

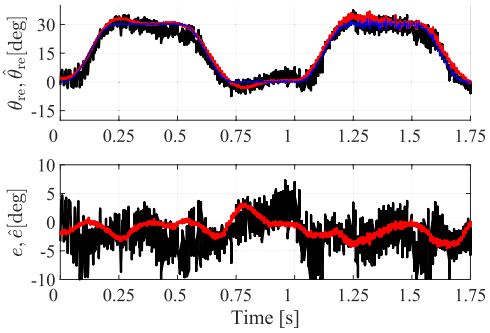

(d) with all proposed strategies.

Fig. 11. Experimental results of positioning control (T = 250 ms)

differential calculation and the τ_d calculation, and (d) with all proposed strategies. In the upper figures of (a) to (d) in Figs. 10 and 11, $\theta^*_{re}[k]$, $\theta_{re}[k]$ and $\hat{\theta}_{re}[k]$ are shown in the blue, red and black lines, respectively. In the lower figures of (a) to (d) in Figs. 10 and 11, $e[k] := \theta^*_{re}[k] - \theta_{re}[k]$ and $\hat{e}[k] := \hat{\theta}_{re}[k] - \theta_{re}[k]$ are shown in the red and black lines, respectively. Table 3 lists each tracking error and estimation error of each result in Figs. 10 and 11. In Table 3, The tracking error in transient state is evaluated by the following criteria:

$$J_{ts} := \max_{k \in T_{1,1} \cup T_{3,1} \ldots} |e[k]| \cdots\cdots\cdots\cdots\cdots\cdots\cdots\cdots (24)$$

The tracking error in steady state is evaluated by the following criteria:

$$J_{ss} := \frac{1}{T_{ss}} \sum_{k \in T_{2,1} \cup T_{4,1}, \ldots} e^2[k] \cdots\cdots\cdots\cdots\cdots\cdots\cdots (25)$$

where T_{ss} is sum of the period of steady state.

Table 3. Evaluation of experimental results

	T = 500 ms				T = 250 ms			
Evaluation	(a)	(b)	(c)	(d)	(a)	(b)	(c)	(d)
J_{ts}	6.2	4.8	3.6	3.6	8.8	6.8	4.8	4.5
J_{ss}	7.2	3.3	1.5	3.9	10.0	10.9	1.6	2.2
J_{ee}	9.2	7.6	8.8	11.4	7.2	7.0	12.0	11.4

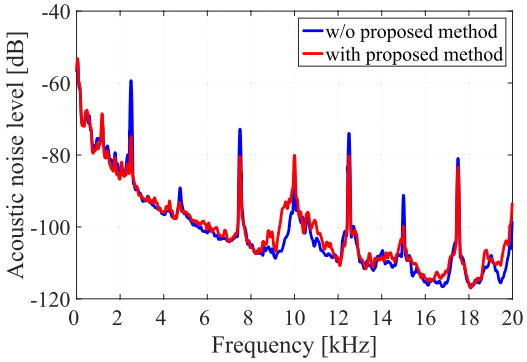

Fig. 12. Acoustic noise level

The estimation error in the transient state is evaluated by the following criteria:

$$J_{ee} := \max_k |\hat{e}[k]| \quad \cdots\cdots (26)$$

From Table 3, we can see that J_{ts} (the tracking errors in transient state) of (b) are less than those of (a), which validates the effectiveness of the proposed differential calculation in both cases of T = 500 ms and T = 250 ms.

We can also see that J_{ss} (the tracking errors in steady state) of (c) are less than those of (b) as listed in Table 3. This is because the disturbance torque τ_d is considered in (c).

From Table 3, we can also see that J_{ee} (the estimation error in transient state) of (d) is larger than that of (c) when T = 500 ms. Nevertheless, note that little difference exists in J_{ts} (the tracking error in transient state) between (c) and (d), as listed in Table 3.

Figure 12 shows the measured acoustic noise levels when the proposed high-frequency voltage injection strategy is applied to the positioning control when T = 500 ms. From Fig. 12, we can observe that the the acoustic noise level is effectively suppressed by 16.0 dB in 2.5 kHz by using our high-frequency voltage injection strategy. It should be also noted that there exists little difference in the tracking control errors between (c) and (d) as listed in Table 3.

These results validate the effectiveness of the position sensorless adaptive positioning servo system with the proposed simplified differential calculation and high-frequency voltage injection for acoustic noise suppression from the perspectives of tracking control performance and acoustic noise suppression.

5. Conclusion

In this paper, we addressed a position sensorless adaptive positioning servo system. For the system, a convolutional integration-based second-order differential calculation was applied to the identification of augmented parameters in the adaptive scheme. In addition, we also proposed a high-frequency voltage injection, considering the trade-off between the acoustic noise suppression and the estimation performance.

The effectiveness of the proposed strategies: the second-order differential calculation of the identified parameters, and the high-frequency voltage injection were verified through experiments. From the experimental results, we concluded that highly accurate positioning control could be successfully achieved, in which the position control error was less than 4.5° for the moving time T = 250 ms. In addition, the acoustic noise level could be sufficiently suppressed by the proposed variable amplitude strategy while satisfying the acceptable control performance.

Acknowledgment

This work is supported by MEXT KAKENHI Grant numbered 15K05960. The authors would like to express gratitude for the financial support.

References

(1) S. Ogasawara and H. Akagi: “Implementation and application control performance of a position-sensorless IPM motor drive system based on magnetic saliency”, *IEEE Trans. Ind. Appl.*, Vol.34, No.4, pp.806–812 (1998)

(2) S. Sato and K. Ide: “Application Trends of Sensorless AC Motor Drives in Europe”, *IEEE Trans. Ind. Appl.*, Vol.3, No.2, pp.97–103 (2014)

(3) O.C. Ferreira and R. Kennel: “Encoderless Control of Industrial Servo Drives”, in *Proc. of 12th International Power Electronics and Motion Control Conference*, pp.1962–1967, Portoroz, Slovenia (2009)

(4) F. Cupertino, G. Pellegrino, P. Giangrande, and L. Salvatore: “Sensorless position control of Permanent-Magnet Motors With Pulsating Current Injection and Compensation of Motor End Effects”, *IEEE Trans. Ind. Appl.*, Vol.47, No.3, pp.1371–1379 (2011)

(5) S. Murakami, T. Shiota, M.O.K. Ide, and M. Hisatsune: “Encoderless Servo Drive With Adequately Designed IPMSM for Pulse-Voltage-Injection-Based Position Detection”, *IEEE Trans. Ind. Appl.*, Vol.48, No.6, pp.1922–1930 (2012)

(6) M. Asada, M. Hasegawa, and K. Matsui: “Adaptive positioning control of servo systems based on simple adaptive control”, in *Proc. of International Conference on Electrical Engineering* (*ICEE*), Busan, Korea, pS-ADM-02 (2010)

(7) M. Sawada and K. Itamiya: “An Improvement of Transient Response of Dynamic Certainty Equivalent Model Reference Adaptive Control System Based on New Smooth Parameter Projection High Order Tuner”, *SICE journal of control, Measurement, and System Integration*, Vol.6, No.4, pp.243–251 (2013)

(8) N. Kawamura, M. Hasegawa, K.Z. Liu, and T. Zanma: “Position-sensorless adaptive positioning control system for ipmsms”, *IET Electric Power Applications*, Vol.13, No.2, pp.138–146 (2019)

(9) R. Ortega: “On Morse’s New Adaptive Controller: Parameter Convergence and Transient Performance”, *IEEE Trans. Autom. Control*, Vol.47, No.3, pp.1191–1202 (1993)

(10) J. Kertzscher: “Ein Verfahren zur Identifikation der elektrischen Parameter von Asynchronmachinen”, Ph.D. dissertation, TU Bergakademie Freiberg (2003)

(11) A. Uphues, K. Notzold, R. Wegener, and S. Soter: “Comparison of parameter identification approaches with linearised process models based on RLS for induction machines with P>100 kW”, in *Proc. of International Conference on Industrial Technology* (*ICIT*), pp.134–140, Taipei, Taiwan (2016)

(12) N. Kawamura and M. Hasegawa: “Position sensorless adaptive positioning servo system based on DyCE principle with adaptive control input synthesis using convolutional integration for differential calculation”, in *Proc. of 2017 International Conference on Power Electronics and Drive Systems* (*PEDS*), pp.837–842, Honolulu, HI, USA (2017)

(13) N. Kawamura and M. Hasegawa: “Suppression of Acoustic Noise of Position Sensorless Adaptive Positioning Servo System Based on DyCE Principle”, in *Proc. of 2018 International Symposium on Power Electronics, Electrical Drives, Automation and Motion* (*SPEEDAM*), pp.907–912, Amalfi, Italy (2018)

(14) J.I. Ha and S.K. Sul: “Sensorless Field-Orientation Control of an Induction Machine by High-Frequency Signal Injection”, *IEEE Trans. Ind. Appl.*, Vol.35, No.1, pp.45–51 (1999)

(15) Y.D. Yoon, S.K. Sul, S. Morimoto, and K. Ide: “High Bandwidth Sensorless

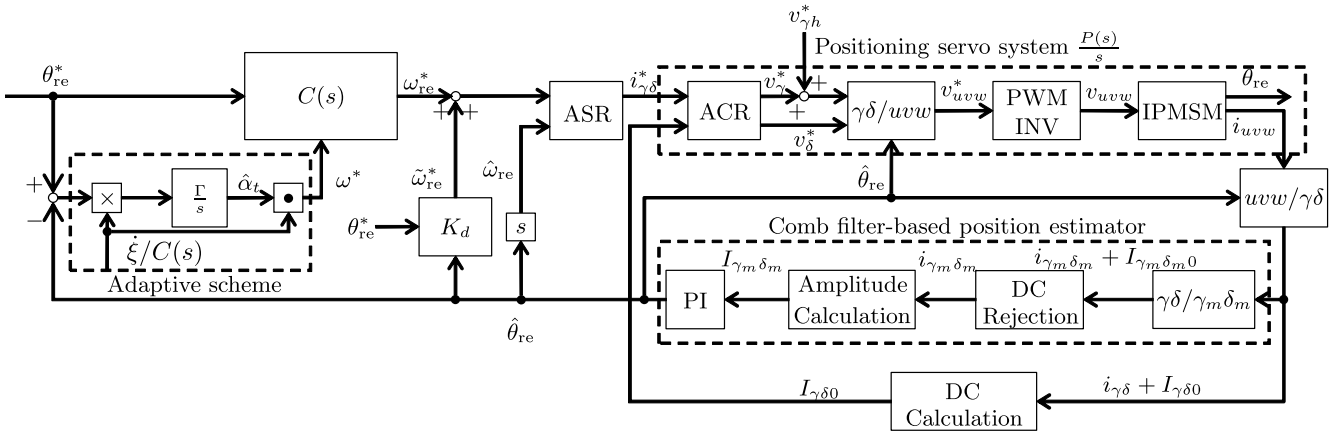

app. Fig. 1. Block diagram of position sensorless adaptive positioning servo system with ASR [6][8]

Algorithm for AC Machines Based on Square-wave Type Voltage Injection", *IEEE Trans. Ind. Appl.*, Vol.47, No.3, pp.2123–2130 (2011)

(16) Z. Chen, M. Tomita, S. Doki, and S. Okuma: "An Extended Electromotive Force Model for Sensorless Control of Interior Permanent Magnet Synchronous Motors", *IEEE Trans. Ind. Electron.*, Vol.50, No.2, pp.288–295 (2013)

(17) S. Taniguchi, S. Wakao, K. Kondo, and T. Yoneyama: "Position sensorless control of permanent magnet synchronous motor at low speed range using harmonic voltage injection", in *Proc. of 2007 European Conference on Power Electronics and Applications*, Aalborg, Denmark (2007)

(18) A.R. Setty, S. Wekhande, and K. Chatterjee: "Adaptive signal amplitude for high frequency signal injection based sensorless PMSM drives", in *Proc. of Sensorless Control for Electrical Drives and Predictive Control of Electrical Drives and Power Electronics* (*SLED/PRECEDE*), pp.1–5, Munich, Germany (2013)

(19) H. Jiang and M. Sumner: "Sensorless torque control of a PM motor using modified HF injection method for audible noise reduction", in *Proc. of European Conference on Power Electronics and Applications* (*EPE*), pp.1–8, Birmingham, UK (2011)

(20) S. Taniguchi, K. Yasui, and K. Yuki: "Noise Reduction Method by Injected Frequency Control for Position Sensorless Control of Permanent Magnet Synchronous Motor", in *Proc. of International Power Electronics Conference* (*IPEC*), pp.2465–2469, Hiroshima, Japan (2014)

(21) S. Sato, H. Iura, K. Ide, and S.K. Sul: "Three Years of Industrial Experience with Sensorless IPMSM Drive based on High Frequency Injection Method", in *Proc. of IEEE International Symposium on Sensorless Control for Electrical Drives* (*SLED*), pp.74–79, Birmingham, UK (2011)

(22) T. Suzuki, M. Hasegawa, M. Tomita, and S. Doki: "Initial position estimation for IPMSMs using comb filters and effects on various injected signal frequencies", *IEEJ Trans. Ind. Appl.*, Vol.4, No.3, pp.204–211 (2015)

(23) M. Vidyasagar: *Nonlinear systems Analysis*, 2nd ed. Upper Saddle River, NJ, USA: Prentice-Hall International (2002)

(24) P.A. Ioannou and J. Sun: *Robust adaptive control*. Upper Saddle River, NJ, USA: Prentice-Hall International (1996)

Appendix

The earlier positioning control systems [6][8] are shown in app. Fig. 1. In app. Fig. 1, the PI-type ASR is given as $K_{Ps} + \frac{K_{Is}}{s}$ ($K_{Ps}, K_{Is} > 0$). To discuss the relationship between the ASR shown in app. Fig. 1, and the APR shown in Fig. 1, we set $K_d = 0$ ($\tilde{\omega}^*_{\rm re} = 0$) since K_d is used for only the drift compensation which is not related to the discussion. In app. Fig. 1, focusing on the ASR, and defining the rotor speed control error as $\Delta\omega_{\rm re} = \omega^*_{\rm re} - \hat{\omega}_{\rm re}$, we obtain the δ-axis current reference i^*_δ as follows:

$$i^*_\delta = \left(K_{Ps} + \frac{K_{Is}}{s}\right)\Delta\omega_{\rm re} \cdots\cdots\cdots\cdots\cdots\cdots\cdots\cdots \text{(A1)}$$

$$= (sK_{Ps} + K_{Is})\left(\frac{\Delta\omega_{\rm re}}{s}\right) \cdots\cdots\cdots\cdots\cdots\cdots\cdots\cdots \text{(A2)}$$

$$= (sK_D + K_P)\,\Delta\theta_{\rm re} \cdots\cdots\cdots\cdots\cdots\cdots\cdots\cdots \text{(A3)}$$

$$= K_D\Delta\omega_{\rm re} + K_P\Delta\theta_{\rm re}, \cdots\cdots\cdots\cdots\cdots\cdots\cdots\cdots \text{(A4)}$$

where $K_D = K_{Ps}$ and $K_P = K_{Is}$. Thus, the APR shown in Fig. 1 is $(sK_D + K_P)$ from (A3) formally. Note that $\Delta\omega_{\rm re}$ is obtained without differentiating $\Delta\theta_{\rm re}$. Therefore, from (A4), i^*_δ can be generated without integral operation compared with (A1). Even if the ASR in app. Fig. 1 is simply replaced by the APR shown in Fig. 1, the control performance depends on the time constant of the resulting APR. For this reason, the adaptive scheme is introduced to generate the direct input to the ACR, and the APR is used subsidiarily for the high-speed positioning control in our positioning servo system shown in Fig. 1. Thus, the control performance is characterized by the time constant of the ACR once the parameters are successfully identified.

Naoki Kawamura (Student Member) received the B.Eng., and M.Eng., degrees in electrical engineering from Chubu University, Aichi, Japan, in 2016 and 2018, respectively, where he is currently working toward the Ph.D. degree from Chiba University, Chiba, Japan. His research interests is the area of power electronics, especially, motor drives. He received the IEEJ Excellent Presentation Award from Motor Drive Technical Meeting 2018. Mr. Kawamura is a student member of the IEEE.

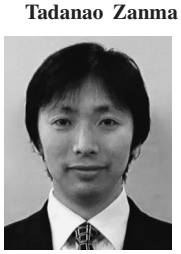

Tadanao Zanma (Senior Member) received the B. Eng., M. Eng., and Ph.D. from Nagoya University in 1995, 1997 and 2000, respectively, all in Electrical Engineering. From 2000 to 2007, he was with Mie University initially as a Research Associate, and since 2007, as an Assistant Professor. In 2007, he was an academic guest in ETH Zurich. He was an Associate Professor in Mie University from 2009 to 2011. He has been with Chiba University as an Associate Professor since 2011. His current research interests include hybrid dynamical control, switched systems, networked control systems, especially, system control based on mixed logical dynamical systems and model predictive control. He has received FANUC FA and Robot Foundation thesis prize in 2009, and IEEJ Distinguished Paper Award 2010 and 2015. He is a member of SICE, ISCIE and IEEE.

Kenta Koiwa (Member) received the B.E. and M.E. degrees in electrical engineering from the Kitami Institute of Technology, Japan, in 2012 and 2014, respectively, and the Ph.D. degree in electrical engineering from Chiba University, Japan, in 2017, where he has been an Assistant Professor with the Department of Electrical and Electronic Engineering. His research interests include power systems, renewable energy, and power electronics.

Kang-Zhi Liu (Member) received his B.E. degree from Northwestern Polytechnical University of China in 1984, M.E. and Ph.D. degrees from Chiba University of Japan in 1988 and 1991. Then, he joined Chiba University and is now a Professor. His main fields are control theory, power system, smart grid and electrical drives. He has authored six books, received a Young Author Award and three Best Paper Awards from SICE, Japan. He served as a director of SICE, Japan in 2017 and 2018.

Masaru Hasegawa (Senior Member) received the B.Eng., M.Eng., and Ph.D. degrees in electrical engineering from Nagoya University, Japan, in 1996, 1998, and 2001, respectively. Since 2013, he has been a Professor at Chubu University, Japan. His research interests are in the area of control theory and application to power electronics and motor drives. He received the Paper Awards from Fanuc FA and Robot Foundation, IEEJ Distinguished Paper Award 2017 and IEEE-IECON'03 Presentation Award. Prof. Hasegawa is a member of the IEEE.